Structural and magnetic studies of mononuclear lanthanide complexes derived from N-rich chiral Schiff bases†

E. Pilichos,[a] M. Font-Bardia, [b] A. Escuer [*a] and J. Mayans[*c]

[a]Departament de Química Inorgànica i Orgànica, Secció Inorgànica and Institute of Nanoscience (IN2UB) and Nanotecnology, Universitat de Barcelona, Marti i Franques 1-11, Barcelona-08028, Spain. E-mail: albert.escuer@qi.ub.edu

[b]Departament de Mineralogia, Cristal·lografia i Dipòsits Minerals and Unitat de Difracció de R-X, Centre Científic i Tecnològic de la Universitat de Barcelona (CCiTUB), Universitat de Barcelona, Solé i Sabarís 1-3, 08028 Barcelona, Spain

[c]Instituto de Ciencia Molecular (ICMol), Universidad de Valencia, Catedrático José Beltran 2, 46980 Paterna, Valencia, Spain. E-mail: julia.mayans@uv.es

ABSTRACT

A new family of mononuclear lanthanide complexes with the formula $[Ce^{III}(L)(NO_3)_3(MeOH)]$ (1) and $[Ln^{III}(L)(NO_3)_3]\cdot MeOH$ where Ln = Gd (2) or Dy (3) and L = N,N'-bis(pyridin-2-ylmethylene)cyclohexane-1,2-diamine has been obtained with the use of enantiomerically pure Schiff bases. Dynamic magnetic studies indicate that 1–3 present field-induced slow relaxation of the magnetization and their response has been compared with the magnetically diluted complexes 2d and 3d. Structural studies have been carried out by single crystal X-ray and powder diffraction.

INTRODUCTION

The coordination chemistry of lanthanide(III) ions has recently attracted the interest of the scientific community for different reasons like their ability to form oligo- and polynuclear metal complexes (coordination clusters) with unique and aesthetically attractive structures, their unusual luminescence properties resulting from the forbidden f–f electronic transitions that emerge when organic ligands are coordinated with 4f metal ions, the so-called antenna effect, and their essential role in the development of efficient single-molecule magnets (SMMs) due to their single-ion anisotropy.[1–3] The discovery by Ishikawa and co-workers[4] that a terbium–phthalocyaninate complex is magnetically bistable up to 30 K opened a new horizon in the field of molecular magnetism and offered a wide pathway for new studies. It was soon realized that this remarkable magnetic behaviour is attributed to the large magnetic moment of Tb^{III} ($^7F_6$ in the ground state) and to the strong easy axis type single ion anisotropy which it assumes in a specific coordination environment. This leads to a large effective anisotropy energy barrier, U_{eff}, for the reversal of the magnetization. However, in the past few years, many reports pointed out that the presence of a large anisotropy barrier is not enough to increase the relaxation time in all the temperature range, because of the competition between relaxation processes, e.g. Raman and direct one.[5,6]

Among this, the capricious geometries around the lanthanide(III) spin carrier in these molecular systems result in the apparition of rhombic anisotropy (E) which allows the occurrence of quantum tunneling of magnetization (QTM) relaxation which compromises their efficiency as SMMs.[7–9]

To date, many lanthanide coordination complexes have been reported to show slow relaxation of the magnetization, as probed by ac measurements using a SQUID magnetometer, either with or without the presence of an external applied field. Among lanthanide-derived systems, complexes based on Dy^{III} have been the most studied cases due to its large magnetic moment ($^6H_{15/2}$ in the ground state) and due to its Kramers ion nature, which ensures the degeneracy of the two lowest lying levels and reduces the possibility of QTM.[9–13] However, any paramagnetic lanthanide(III) ion (Eu^{III} is the exception because of its non-magnetic ground state, $^7F_0$) can show slow relaxation of the magnetization under appropriate conditions as was proposed recently by Rinehart et al.,[14] who postulated a qualitative model where the electronic density around the lanthanide ion plays a pivotal role which could effectively enhance the singleion anisotropy. Following this approach, many publications can be found in the literature with the so called “uncommon lanthanides” in molecular magnetism, which include the light lanthanides Ce^{III} and Nd^{III} with low magnetic moments, but also the non-Kramers Ho^{III} or Yb^{III}, for which, even its high anisotropic character, a scarce number of SMMs have been reported.[15]

Taking into advantage our previous experience on the chemistry of compartmental and tetradentate Schiff bases with lanthanides,[16,17] we synthesized a new family of mononuclear lanthanide complexes with the formula $[Ce^{III}(L)(NO3)3(MeOH)]$ (1) and $[Ln^{III}(L)(NO_3)_3]\cdot MeOH$ for Ln = Gd (2) and Dy (3) in which L = N,N’-bis(pyridin-2-ylmethylene)cyclohexane-1,2-diamine (Chart 1), obtained by the reaction of the L Schiff base with lanthanide nitrates in methanolic solution. The magnetic dilutions of 2 and 3 Gd@Eu (2b) and Dy@Eu (3b) were also performed to compare the effect of dilution with Eu^{III} of an isotropic and an anisotropic lanthanide(III) ion in a Ln^{III}/Eu^{III} ratio of $\sim$ 0.2 : 0.8.

The organic chiral ligand L was synthesized by the condensation of two equivalents of 2-pyridinecarboxaldehyde and 1 equivalent of (1R/S,2R/S)-1,2-diamino cyclohexane in methanolic solution. Neutral N-rich Schiff bases (N4L) have been less employed than the more usual O-rich Schiff bases derived from salicylic or o-vanillin precursors and complexes with the general formula $[Ln(N_4\text{-}L)(NO_3)_3]$ or $[Ln(N_4\text{-}L)(Cl)_3]$ have been studied from structural,[18–21] catalytic[22] and luminescence23,24 points of view. However, their magnetic properties remain practically unexplored.[17,25]

Complexes 1–3 have been magnetically studied and the dynamic magnetic measurements revealed that they present field-induced slow relaxation of the magnetization. These results were expected for the highly anisotropic Dy^{III} derivative with a high magnetic moment, but demonstrate that Ce^{III}, with its lonely 4f electron ($^2F_{5/2}$ in the ground state), which yields a low magnetic moment, allows enough spin–orbit coupling to present relevant magnetic anisotropy of its ground J = 5/2 state, is not that "uncommon" as a building block for field-induced SMMs[15,25–27] and that also the non-anisotropic member of the lanthanide family, Gd^{III}, is becoming a regular source of SMM systems.[28–34] The effect of magnetic dilution on the relaxation mechanisms for an isotropic cation (Gd^{III} (2)) and one isostructural anisotropic system (Dy^{III} (3)) has been studied by comparison of the out-of-phase response of the diluted compounds 2d and 3d.

EXPERIMENTAL

X-ray crystallography

Single crystal structural determination was selectively performed for the complexes that exhibit ac response. Colourless prism-like specimens of 1SS, 2SS and 3RS were used for the X-ray crystallographic analysis. The X-ray intensity data were collected using a D8 Venture system equipped with a multilayer monochromator and a Mo microfocus (λ = 0.71073 Å).

The frames were integrated with the Bruker SAINT software package using a narrow-frame algorithm. The structure was solved and refined using the Bruker SHELXTL Software Package.[35] Crystal data and refinement details are summarized in Table 1. Further crystallographic details can be found in the corresponding CIF files provided in the ESI.†

Powder X-ray diffraction was performed with a PANalytical X'Pert PRO MPD θ/θ powder diffractometer of 240 millimetres of radius, in a configuration of convergent beam with a focalizing mirror and a transmission geometry with flat samples sandwiched between low absorbing films and Cu Kα radiation (λ = 1.5418 Å). Comparison between the calculated spectrum from the single crystal structure of 2 and the experimental spectra for the diluted compounds 2d and 3d confirms the isostructurality among them, Fig. S1.†

Physical measurements

Magnetic susceptibility measurements were carried out on pressed polycrystalline samples with a MPMS5 Quantum Design susceptometer working in the range 30–300 K under a magnetic field of 0.3 T and under a field of 0.03 T in the 30–2 K range to avoid saturation effects at low temperature. Diamagnetic corrections were estimated from Pascal tables. Infrared spectra (4000–400 cm^{-1}) were recorded from KBr pellets on a Bruker IFS-125 FT-IR spectrophotometer. ECD spectra were recorded in methanolic solutions using a Jasco-815 spectropolarimeter.

Syntheses

L ligand . The synthesis was accomplished by reaction of 2-pyridincarboxaldehyde (0.107 g per mmol) and the corresponding isomer of 1,2-diaminocyclohexane (0.057 g per 0.5 mmol) dissolved in 10 mL of MeOH and kept with continuous stirring for 30 minutes at room temperature. The dissolution was employed directly to synthesize the derived complexes without isolation of the solid ligand. Similar syntheses were previously reported.[17,36]

$[Ce(L)(NO_3)_3(MeOH)]$ (1) and $[Ln(L)(NO_3)_3]\cdot MeOH$, Ln = Gd (2) and Dy (3). The corresponding lanthanide nitrate salt (0.5 mmol) was added to the previously prepared ligand. The resulting solution was left under stirring for two hours at room temperature. The complexes precipitate as a yellow powder that was collected in high yield (∼70%), filtered and washed with cold diethylether (2 × 3 mL). Yellowish prism-like crystals suitable for X-ray diffraction were obtained after a few days by layering the filtrate with diethylether.

The diluted complexes 2d and 3d were prepared following the same procedure but starting from europium nitrate and gadolinium or dysprosium nitrate (0.4 : 0.1 mmol).

The cation ratio for the diluted complexes was determined from the comparison of their magnetic moments resulting in $Eu_{0.84}Gd_{0.16}$ and $Eu_{0.82}Dy_{0.18}$ for 2d and 3d, respectively.

Calculated/found elemental analysis for 1 C, 35.08/35.2; N, 15.07/15.1; H, 3.72/3.8%; for 2 C, 34.17/34.0; N, 14.68/14.5; H, 3.62/3.7%; for 3 C, 33.91/34.1; N, 14.57/14.4; H, 3.59/3.6%. Selected IR peaks for all compounds (KBr, cm^{-1}): 3400(b), 2937(w), 1647(m), 1595(s), 1483(s), 1384(s), 1017(m), 782(m), 636(m), ESI, Fig. S2.†

RESULTS AND DISCUSSION

Description of the structures

The structures of the complexes 1SS, 2SS and 3RS were determined by single crystal X-ray diffraction. The Gd^{III} and Dy^{III} complexes are isostructural and to avoid repetitive text only the GdIII compound will be described.

[Ce(L)(NO3)3(MeOH)] (1SS). A partially labelled plot of 1SS is shown in Fig. 1 top. Selected bond parameters and angles are summarized in Table 2. The structure of 1SS consists of a neutral mononuclear complex of Ce^{III}, in which the cation links one neutral tetradentate L ligand, three bidentate nitrato ligands and one methanol molecule, resulting in an 11-coordinated environment.

The four N-donor atoms from the organic ligand L are coordinated to the central cation with Ce–N bond distances in the narrow 2.657(3)–2.721(3) Å range. Three bidentate chelate nitrato and the methanol ligands complete the coordination sphere of the cation with Ce–O bond distances comprising between 2.555(2) and 2.733(2) Å. The Ce^{III} environment is severely distorted due to the low bite angle of the organic ligand and the nitrato groups: the N–Ce–N bond angles between the neighbouring N-donors show values comprised between 62.30(9) and 59.99(8)° and the O–Ce–O bond angles for each nitrate are close to 48°. SHAPE[37] calculations indicate that the closer coordination polyhedron around the Ce^{III} cation is an intermediate between the ideal C_{5v} capped pentagonal prism and antiprism (Fig. 1 and Table S1†) with a large CShM due to the strong distortion generated by the low bite of the nitrato ligands and the neighbour N-donor atoms from the Schiff base.

The molecules are well isolated in the network (a minimum Ce···Ce distance of 8.506(1) Å), the only intermolecular contacts being the weak CH···O H-bonds established between the aromatic rings and the O-atoms from the nitrato ligands of the neighbouring molecules.

[Gd(L)(NO$_3$)$_3$]·MeOH (2SS) and [Dy(L)(NO$_3$)$_3$]·MeOH (3RS). A partially labelled plot of 2SS is shown in Fig. 1, bottom. Selected bond parameters and angles for 2SS and 3RS are summarized in Table 2. The structure of 2SS consists of a mononuclear neutral Gd^{III} complex which crystallized in the P1 triclinic system. The unit cell contains two crystallographically non-equivalent molecules (labelled A and B) with slight deviations in bond parameters and angles. The discussion of the structural details will be referred to molecule A. The structure of 2SS consists of neutral mononuclear complexes of Gd^{III}, in which the cations link one tetradentate L ligand and three bidentate nitrato ligands, resulting in a decacoordinated environment. The four N-donor atoms from the organic ligand L are coordinated to the central metal ion with Gd–N bond distances ranging from 2.506(4) to 2.604(6) Å. Gd–O bond distances are comprised between 2.454(5) and 2.540(4) Å, slightly shorter than the Gd–N ones. The Gd^{III} environment is also distorted: the N–Gd–N bond angles between the neighbouring N-donors show values around 64° and the O–Gd–O bond angles for each nitrate are close to 51°. SHAPE[37] calculations indicate that the closer coordination polyhedron around the Gd^{III} cation is an ideal sphenocorona (Fig. 1) (C_{2v}, CShM = 3.05, Table S1†) with a relatively large CShM.

Because of the presence of methanol solvent and the accessible O-donors from the nitrate groups, there are intermolecular H-bonds promoted by MeOH···$O_{nitrate}$ contacts with O···O distances in the range of 2.8–2.9 Å. The structure does not present direct contacts

between the complexes and the minimal intercluster Gd···Gd distance is 8.085(1) Å showing a good isolation of the clusters.

The comparison between the three structures shows the gradation of the bond distances according to the reduction of the cationic radius from Ce^{III} to Dy^{III}. For complexes 2 and 3, two nitrato ligands are placed in an axial arrangement, roughly perpendicular to the Schiff base main plane, whereas the addition of an extra ligand (MeOH) in the coordination sphere of the Ce^{III} complex displaces one of the nitrato ligands and this steric hindrance induces the folding of the ligand resulting in a dihedral angle of 145.9(3)° between the aromatic rings, Fig. 2. This distortion displaces the Ce^{III} cation 0.878(1) Å out of the plane defined by the four N-donors of the organic ligand.

Electronic circular dichroism

Chirality transfer is a common feature when using enantiopure chiral ligands in coordination compounds;[38–40] however, transference of chirality from the chiral ligand to the metallic centres is poor in this case and the differences around the lanthanide cation are limited to the relative torsion of the nitrato groups and thus, the chiroptical properties must be mainly related to the ligands due to the π–π* transitions of the aromatic rings as was reported for the related complexes [Ln (L')Cl_3] (L' = N,N'-bis((1,2-diphenyl-(pyridine-2-yl)methylene)-(R,R/S,S)-ethane-1,2-diamine).[17] ECD spectra in methanolic solution were recorded for the representative enantiomeric pairs of 2RR and 2SS, respectively, Fig. 3 and their mirror image confirms the enantiomeric nature of the reported complexes. The spectrum exhibits a positive Cotton effect at λ_{max} = 295, 287(sh) and 246 nm and a negative band at 270 nm for 2RR and the same bands with opposite sign for 2SS.

Magnetic properties

Static measurements. The magnetic susceptibility measurements for the compounds in the form of $\chi_M T$ product vs. temperature were performed on polycrystalline samples in the range of 2–300 K. On cooling, the $\chi_M T$ values decrease from room temperature for the Ce^{III} complex 1 and below 50 K for the Dy^{III} (3) derivative due to the depopulation of the Stark sublevels of the anisotropic Ln^{III} cations. Magnetization measurements show unsaturated values at the maximum explored field of 5 T, which are in good agreement with the corresponding J and g values, Fig. S3.†

The isotropic Gd^{III} complex (2) ($^8S_{7/2}$, g = 2.00, 7.875 cm^3 mol^{-1} K) shows a Curie law response with a constant $\chi_M T$ value of 7.6 cm3 mol^{-1} K in the full range of temperatures that agrees with the expected value for an S = 7/2 spin. Magnetization tends to the expected value of 7.04Nμβ Fig. 4, left. Reduced magnetization measurements between 1.8 and 6.8 K show superimposable plots indicating negligible anisotropy.

However, susceptibility or magnetization measurements are not adequate to determine weak anisotropy for low spin values as is the case of Gd^{III} (S = 7/2) that in contrast can be precisely determined by means of the more sensitive EPR spectroscopy. The X-band spectra of complex 2 are far from the single g ≈ 2.00 band characteristic of an isotropic cation, showing several absorptions at g = 6.8, 3.1 and 1.69 that can be simulated with a zero field splitting

parameter of 0.07 cm^{-1}, Fig. 4, right. The spectrum for the diluted compound 2d shows the same absorptions with a sharper linewidth as a result of the reduction of the dipolar interactions, confirming the identical environment around the Gd^{III} cation between the pure and diluted complexes, Fig. S4.†

Dynamic measurements. Preliminary alternate current measurements showed that any of the complexes exhibits outof-phase response in zero field. Scan of the response under different applied dc fields (Fig. S5†) revealed defined peaks for the CeI^{II}, Gd^{III} and Dy^{III} complexes.

Frequency-dependent susceptibility for the Ce^{III} compound 1 was analysed by applying a dc field of 0.2 T in the 500–1500 Hz range of frequencies at which complete maxima were defined (Fig. 5 and S6†). An Arrhenius dependency fit was firstly used to calculate the relaxation time (τ_0) and the effective relaxation energy barrier (U_{eff}) by means of the equation

$$\ln(2\pi\omega) = \ln(1/\tau_0) - U_{\text{eff}}/K_{\text{B}}T$$

which supposes the so-called Orbach relaxation which involves two phonons in the spin–lattice relaxation through real states and yield the best fitting values of U_{eff} of 17.0 K and a τ0 value of 3.9×10^{-8} s. Using the data extracted from the fitting of the Argand plot for 1, the relaxation parameters yield a value of 13.6 K and a τ_0 value of 3.2×10^{-7} s, confirming the occurrence of only one relaxation process in this temperature range (Fig. 5 and S7†) with alpha values ranging from 0.16 to 0.34 between 2 and 4 K indicating a wide distribution of the relaxation times of the observed relaxation process. Alternate current susceptibility measurements for the dysprosium derivative 3 were performed under a field of 0.1 T in the 10–1500 Hz range of frequencies showing well-resolved $\chi''_M(T)$ peaks for frequencies above 39 Hz, Fig. 6 left. At low temperature, the χ''_M peaks overlap with a relaxation process effective below 2 K that corresponds to a QTM relaxation. The Arrhenius fit of the peak maxima for the larger frequencies yielded U_{eff} = 30.6 K and $\tau_0 = 7.2 \times 10^{-7}$ s. The ln(τ) vs. T−1 plot shows an almost linear Arrhenius dependence that deviates from linearity at low temperatures in agreement with the presence of a different process. Analysis of the semi-circular Argand plot gives α values ranging between 0.04 and 0.46 (1.8–7.6 K), suggesting a wide distribution of the relaxation times in this temperature range.

Generalized Debye fitting of the relaxation times obtained for the larger temperatures gives the close values of U_{eff} = 30.6 K and $\tau_0 = 9.7 \times 10^{-7}$ s.

In order to analyse the effect of the dipolar interactions in 3, the diluted sample 3d in a $\mathrm{Eu}^{\mathrm{III}}_{0.82}/\mathrm{Dy}^{\mathrm{III}}_{0.18}$ ratio was studied under the same conditions (field 0.1 T, 10–1500 Hz), Fig. 6, right. It is noteworthy that the only difference between the pure and diluted samples was the better definition of the outof-phase peaks in the $\chi''_M(T)$ plot for the whole range of frequencies, including the lower ones, due to the suppression of the low T QTM process. The Arrhenius fit of the $\chi''_M(T)$ peak position of the larger frequencies yielded U_{eff} = 34.6 K and $\tau_0 = 2.4 \times 10^{-7}$ s in agreement with the fit of relaxation times obtained from the ln(t) fit for the larger temperatures of the Argand plot, that gives U_{eff} = 32.4 K and $\tau0 = 4.9 \times 10^{-7}$ s. The α values varying between 0.05 and 0.32 show a shorter variation range than complex 3.

It is important to note that the values of the effective relaxation barrier for complexes 1, 3 and 3d are by far lower than the usual first excited state of the Ln^{III} cation, and an overbarrier relaxation is not allowed which is a common feature in field-induced SMM lanthanide systems meaning that the Orbach process parameters given above can only be taken as a first approach.

It is noteworthy that the Gd^{III} complex 2 and its diluted analogous 2d exhibit strong out-of-phase signals despite its spherical electronic distribution and its a priori isotropic character.

The response of the two systems as a function of the transverse field was studied between 0 and 1 T for selected low (LF, 10 Hz) and high (HF, 1488 Hz) frequencies to choose the optimal field for the $\chi''M(T)$ measurements.

The complexes do not show signals in zero field but the measurements reveal a strong field-dependence, and a continuous shift of the signals for the increasing field with a fast increase of intensity with a maximum around 5000 G, decreasing gradually for larger fields, Fig. 7. Remarkably, this continuous shift differs from the usual response of anisotropic systems for which the shift and intensity of the out-of-phase signals have a limit corresponding to the optimal QTM suppression.

The $\chi''_M(T)$ measurements for 2 in the frequency range of 1–1488 Hz were performed under a field of 4000 G. The $\chi''_M(T)$ plot clearly shows two HF/LF processes with an intermediate region with a minimal signal intensity at around 100 Hz, Fig. 8, left. The HF signal is clearly temperature dependent following an Arrhenius law with a short $\tau_0 = 2.9 \times 10^{-12}$ s and a U_{eff} barrier of 82 K that overcome in orders of magnitude the barrier ($DS^2 - 1/4 = 0.6\ cm^{-1}$) derived from the small D value calculated from EPR measurements. In contrast, the LF peaks are poorly dependent on the frequency. Peak maxima in $\chi''_M(\omega)$ are out of the limits of the recorded frequencies indicating a short relaxation time for the HF process and a large relaxation time for the LF process.

Measurements for the diluted compound 2d show a similar response: HF/LF processes also appear in the $\chi''_M(T)$ plot but shifted to a lower temperature, Fig. 8, right. The temperature dependence of the HF process gives $\tau_0 = 1.9 \times 10^{-8}$ and an U_{eff} barrier of 34 K. As a consequence of the peak shift, the HF process is better defined in the $\chi''_M(\omega)$ plot suggesting larger relaxation times than the concentrated Gd^{III} complex 2. The fit of the relaxation time vs. temperature effectively yields larger τ values for similar U_{eff} values of 13.3 K (2) or 10.6 K (2d).

The isostructurality between the compounds 2, 2d, 3 and 3d allows the comparison in a rigorously identical coordination and network environment between one anisotropic Dy^{III} complex and the analogous Gd^{III} isotropic complexes. Summarizing the above results, Fig. 9, we observed that for the Dy^{III} complex 3 QTM is efficiently suppressed by a magnetic dilution due to the reduction of the dipolar interactions and due to the application of a transverse dc field, whereas the U_{eff} barrier and the relaxation times remain practically unaltered as could be expected for the cation in the same environment.

In contrast, the response of the Gd^{III} system is completely different: the apparent U_{eff} barrier calculated from the maxima of the $\chi''_M(T)$ plot (HF region) is very different from the diluted sample and the analysis of the relaxation times from the fit of the Argand plots shows similar barriers but a clear enlargement of the relaxation times.

SIM response is not expected for a fully isotropic Gd^{III} cation that must behave like a paramagnet but a weak D is induced in a strongly distorted environment. EPR measurements become crucial to determine the D parameter because D values in the 0.1–0.2 cm^{-1} range cannot be detected by susceptibility or magnetization experiments. Low D values are notable to generate conventional SIM/SMM systems because the barrier derived from the double-well takes values around 1 cm^{-1} which are orders of magnitude lower than the experimentally calculated barriers. Thus, QTM and over-barrier relaxation must be excluded meaning that the unusual SIM response for this cation can be related to its weak anisotropy that broke the degeneration of the S = 7/2 level mixing the m_S sublevels under moderate (~0.5 T) external fields. This hypothesis for the origin of the slow relaxation of the magnetization was suggested by S. Gao et al.[30] stating that in the Gd^{III} systems, the D value of 0.1 cm^{-1} allows this separation that the phonon needs to interact with the spin system, promoting a slow relaxation of the magnetization for a quasi-isotropic system. The occurrence of lower or higher values of D enables the apparition of spin–phonon relaxation, and this is what probably occurs in Gd systems which present field-induced slow relaxation of the magnetization.[31,32]

CONCLUSIONS

This paper presents the structure and magnetic characterization of a lanthanide series of complexes built from a Schiff base with a set of four N-donors. The characterization of three new induced SIMs with Dy^{III} and the unusual lanthanide cations Ce^{III} and Gd^{III} is remarkable. Single crystal and powder X-ray diffraction evidence isostructurality between the Dy^{III} and Gd^{III} complexes and with their magnetically diluted analogues. The comparison between the pure $[Ln^{III}(L)(NO_3)_3]$ and the magnetically diluted (Ln^{III}/Eu^{III} ratio ~0.2/0.8) shows the completely different behaviours of two isostructural systems and their dilutions, one derived from a highly anisotropic lanthanide and the other derived from the isotropic one. Even at the end, the result for both cases is the observation of the fingerprint of the SIM response in the ac measurements, the ultimate mechanism through this process is absolutely different for Dy^{III} and Gd^{III} due their opposite natures. This fact emphasizes the need for more detailed studies on Gd^{III} complexes to finally elucidate the ultimate origin of its relaxation, which is until today unexplained.

Conflicts of interest

There are no conflicts to declare.

ACKNOWLEDGMENTS

AE and EP acknowledge the support from MICINN Project PGC2018-094031-B-100. JM acknowledges the support of MICINN project PID2019-109735GB-100 and the Juan de la Cierva Formación postdoctoral grant.

NOTES AND REFERENCES

1 J. Tang and P. Zhang, Lanthanide Single Molecule Magnets, Spriner Berlin Heidelberg, Berlin, Heidelberg, 2016.

2 D. Gatteschi, R. Sessoli and J. Villain, Molecular nanomagnets, Oxford University Press, 2006.

3 L. Sorace, C. Benelli and D. Gatteschi, Chem. Soc. Rev., 2011, 40, 3092.

4 N. Ishikawa, M. Sugita, T. Ishikawa, S. Koshihara and Y. Kaizu, J. Am. Chem. Soc., 2003, 125, 8694.

5 R. J. Blagg, L. Ungur, F. Tuna, J. Speak, P. Comar, D. Collison, W. Wernsdorfer, E. J. L. McInnes, L. F. Chibotaru and R. E. P. Winpenny, Nat. Chem., 2013, 5, 673.

6 W. Wernsdorfer, N. Aliaga-Alcaide, R. Tiron, D. N. Hendrickson and G. Christou, J. Magn. Magn. Mater., 2004, 272–276, 1037.

7 D. Aravena, J. Phys. Chem. Lett., 2018, 9, 5327.

8 S. Hill, S. Datta, J. Liu, R. Inglis, C. J. Milios, P. L. Feng, J. J. Henderson, E. del Barco, E. K. Brechin and D. N. Hendrickson, Dalton Trans., 2010, 39, 4693.

9 P. Zhang, Y.-N. Guo and J. Tang, Coord. Chem. Rev., 2013, 257, 1728.

10 K. Zhang, V. Montigaud, O. Cador, G.-P. Li, B. Le Guennic, J.-K. Tang and Y.-Y. Wang, Inorg. Chem., 2018, 57, 8550.

11 C. A. P. Goodwin, F. Ortu, D. Reta, N. F. Chilton and D. P. Mills, Nature, 2017, 548, 439.

12 Y.-N. Guo, G.-F. Xu, Y. Guo and J. Tang, Dalton Trans., 2011, 40, 9953.

13 F. Ortu, D. Reta, Y.-S. Ding, C. A. P. Goodwin, M. P. Gregson, E. J. K. McInnes, R. E. P. Winpenny, Y.-Z. Zheng, S. T. Liddle, D. P. Mills and N. F. Chilton, Dalton Trans., 2019, 48, 8541.

14 J. D. Rinehart and J. R. Long, Chem. Sci., 2011, 2, 2078.

15 F. Pointillart, O. Cador, B. Le Guennic and L. Ouahab, Coord. Chem. Rev., 2017, 346, 150.

16 J. Mayans, Q. Saéz, M. Font-Bardia and A. Escuer, Dalton Trans., 2019, 48, 641.

17 J. Mayans, L. Sorace, M. Font-Bardia and A. Escuer, Polyhedron, 2019, 270, 264.

18 S. Gourbatsis, J. C. Plakatouras, V. Nastopoulos, C. J. Cardin and N. Hadjiliadis, Inorg. Chem. Commun., 1999, 2, 468.

19 J. Lisowski and J. Mazurek, Polyhedron, 2002, 21, 811.

20 J. Mazurek and J. Lisowski, Polyhedron, 2003, 22, 2877.

21 M. Tsiouri, N. Hadjiliadis, T. Arslan, B. M. Kariuki and J. C. Plakatouras, Inorg. Chem. Commun., 2006, 9, 429.

22 S. Kano, H. Nakano, M. Kojima, N. Baba and K. Nakajima, Inorg. Chim. Acta, 2003, 349, 6.

23 S. Chen, R.-Q. Fan, S. Gao, X. Wang and Y.-L. Yang, J. Lumin., 2013, 149, 75.

24 F. Piccinelli, M. Leonzio, M. Bettinelli, M. Monari, C. Grazioli, A. Melchior and M. Tolazzi, Dalton Trans., 2016, 45, 3310.

25 M. Li, H. Wu, Q. Yang, H. Ke, B. Yin, Q. Shi, W. Wang, Q. Wei, G. Xie and S. Chen, Chem. – Eur. J., 2017, 23, 17775.

26 S. K. Singh, T. Gupta, L. Ungur and G. Rajaraman, Chem. – Eur. J., 2015, 21, 13812.

27 J. J. Le Roy, M. Jeleti, S. I. Gorelsky, I. Korovkov, L. Ungur, L. F. Chibotaru and M. Murugesu, J. Am. Chem. Soc., 2013, 135, 3502.

28 J. J. Le Roy, I. Korovkov, J. E. Kim, E. J. Schelter and M. Murugesu, Dalton Trans., 2014, 43, 2737.

29 R. J. Holmberg, L. T. A. Ho, L. Ungur, I. Korobkov, L. F. Chibotaru and M. Murugesu, Dalton Trans., 2015, 44, 20321.

30 M. Orendáč, L. Sedláková, E. Čižmár, A. Orendáčová, A. Feher, S. A. Zvyagin, J. Wosnitza, W. H. Zhu, Z. M. Wang and S. Gao, Phys. Rev. B: Condens. Matter Mater. Phys., 2010, 81, 214410.

31 A. Vráblová, M. Tomás, L. R. Falvello, L. Dlháň, J. Titiš, J. Černák and R. Boča, Dalton Trans., 2019, 48, 13943.

32 Y. Horii, K. Katoh, Y. Miyazaki, M. Damjanovic, T. Sato, L. Ungur, L. F. Chibotaru, B. K. Breedlove, M. Nakano, W. Wernsdorfer and M. Yamashita, Chem. – Eur. J., 2020, 26, 8076.

33 J. Mayans and A. Escuer, Chem. Commun., 2021, DOI: 10.1039/D0CC07474H, WEB published.

34 T. Ghosh, S. Maity, J. Mayans and A. Ghosh, Inorg. Chem., 2021, DOI: 10.1021/acs.inorgchem.0c03129, WEB published.

35 G. M. Sheldrick, SHELXL-2014/7: Program for the Solution of Crystal Structures, University of Göttingen, Göttingen, Germany, 2014.

36 C. M. Che, W. T. Tang and C. K. Li, J. Chem. Soc., Dalton Trans., 1990, 3735.

37 M. Llunell, D. Casanova, J. Cirera, P. Alemany and S. Alvarez, SHAPE version 2.0, Barcelona, 2010. The program can be obtained by request to the authors.

38 J. Crassous, Chem. Soc. Rev., 2009, 38, 830.

39 H. Miyake, Symmetry, 2014, 6, 880.

40 M. Liu, L. Zhang and T. Wang, Chem. Rev., 2015, 115, 7304.

Table 1 Crystal data, collection and structure refinement details for the X-ray structure determination of complexes 1SS, 2SS and 3RS

	1*SS*	2*SS*	3*RS*
Formula	$C_{19}H_{24}CeN_7O_{10}$	$C_{19}H_{24}GdN_7O_{10}$	$C_{19}H_{24}DyN_7O_{10}$
FW	650.57	667.70	672.95
System	Monoclinic	Triclinic	Triclinic
Space group	*P*21	*P*1	*P*1
a/Å	8.5057(6)	9.5580(9)	9.5045(8)
b/Å	15.531(1)	11.459(1)	11.409(2)
c/Å	9.3697(7)	11.665(1)	11.664(1)
α/°	90	108.182(3)	108.073(3)
β/°	101.896(3)	90.985(3)	90.811(3)
γ/°	90	91.903(3)	92.020(4)
V/Å^3	1211.2(2)	1212.6(2)	1201.2(2)
Z	2	2	2
T, K	100(2)	100(2)	100(2)
θ range/°	2.447–30.647	3.612–30.624	2.145–30.579
Reflex. collected	24 066	36 000	43 858
Reflex. indep.	7171	13 994	7383
Parameters	335	634	329
λ(MoKα), Å	0.71073	0.71073	0.71073
ρ_{calc}, g cm^{-3}	1.784	1.829	1.861
μ(MoK$_\alpha$), mm^{-1}	1.948	2.803	3.180
Flack parameter	0.007(6)	0.036(1)	—
R	0.0204	0.0183	0.0402
ωR^2	0.0374	0.0429	0.0937

Table 2. Selected bond distances (Å) and angles (°) for complexes 1SS, 2SS and 3RS

FIGURE CAPTIONS

Chart 1 Structural formula of the L ligand employed in this work. Asterisks denote the chiral centres.

Figure 1. Partially labelled plots and the ideal coordination polyhedron vs. real donor sites for the Ce^{III} (1) (top) and Gd^{III} (2) (bottom) complexes. The Dy^{III} complex 3 is isostructural to 2. Colour key for all figures: Ce^{III} orange, Gd^{III} light blue, O red, N navy and C grey.

Figure 2. Axial view of complexes 1 (left) and 2 (right) showing the relative position of the nitrato ligands as a function of the coordination number and the arrangement of the Schiff base.

Figure 3. Solution ECD spectra for the EuIII pair of complexes 2RR (red line) and 2SS (blue line).

Figure 4. Left, reduced magnetization for complex 2 measured between 1.8 and 6.8 K with increments of 1 K. Inset, $\chi_M T$ vs. temperature. Right, the X-band EPR spectrum for complex 2. The dashed line shows the simulated spectrum.

Figure 5. Left, χ''_Mf (T) plots for compound 1. Right, Argand plot for 1, (solid lines show the fit of the experimental data).

Figure 6. Dependence of out-of-phase susceptibility for complexes 3 (left) and the diluted compound 3d (right) measured under a dc field of 1000 Oe.

Figure 7. Dependence of LF and HF out-of-phase susceptibility for complex 2 (top) and the diluted compound 2d (down) measured in the field range 0–1.0 T.

Figure 8. Dependence of out-of-phase susceptibility for complexes 2 (left) and the diluted compound 2d (right) measured under a dc field of 4000 Oe.

Figure 9. Top, Arrhenius plot (left) for the HF region from the $\chi''_M(T)$ data and ln(τ) vs. T^{-1} from the Argand plots (right) for the Dy^{III} compounds 3 (black) and 3d (red). Down, the Arrhenius plot (left) for the HF region from the $\chi''_M(T)$ data and ln(t) vs. T^{-1} from the Argand plots (right) for the Gd^{III} compounds 2 (black) and 2d (red).

Chart 1

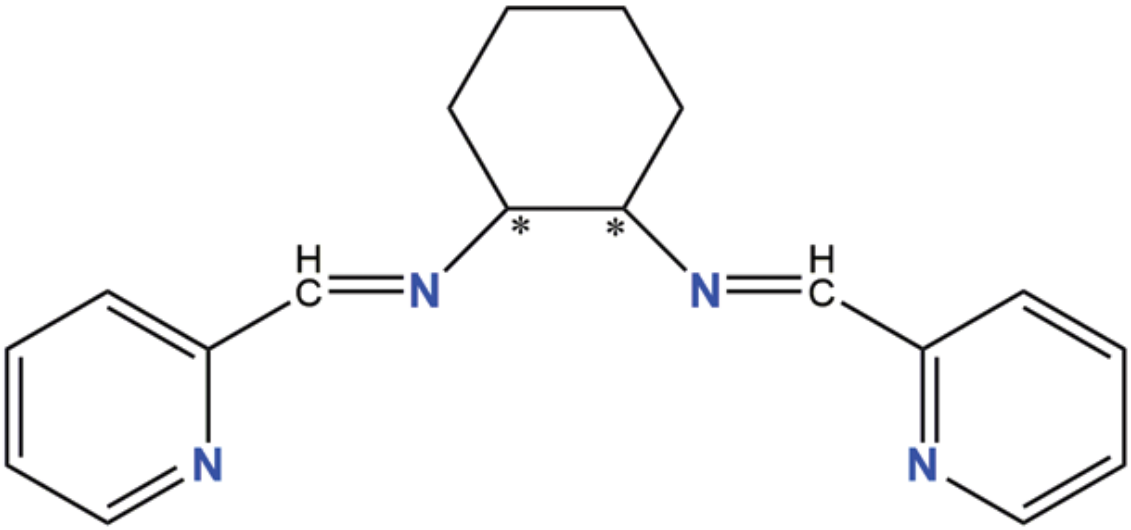

Figure 1.

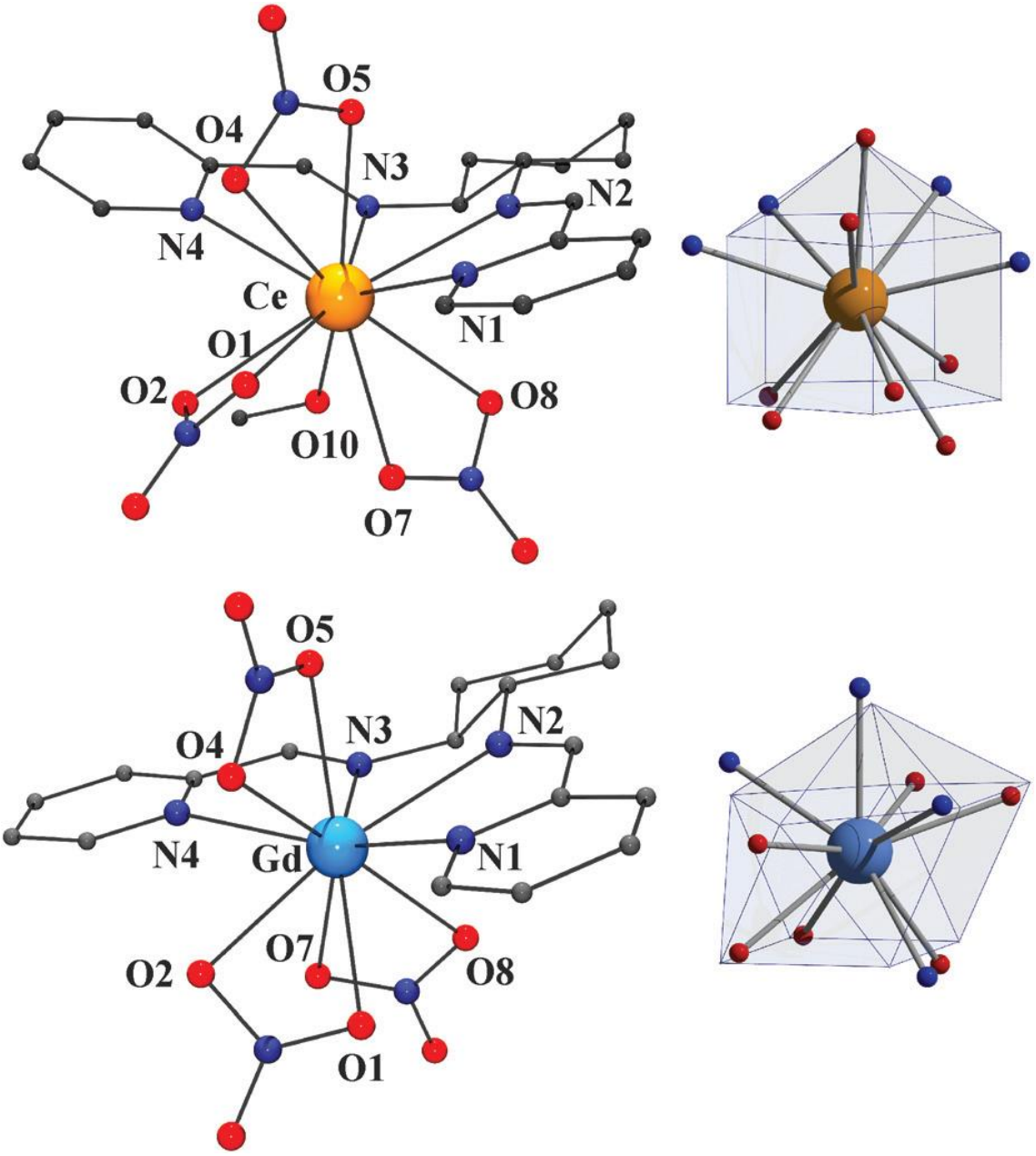

Figure 2.

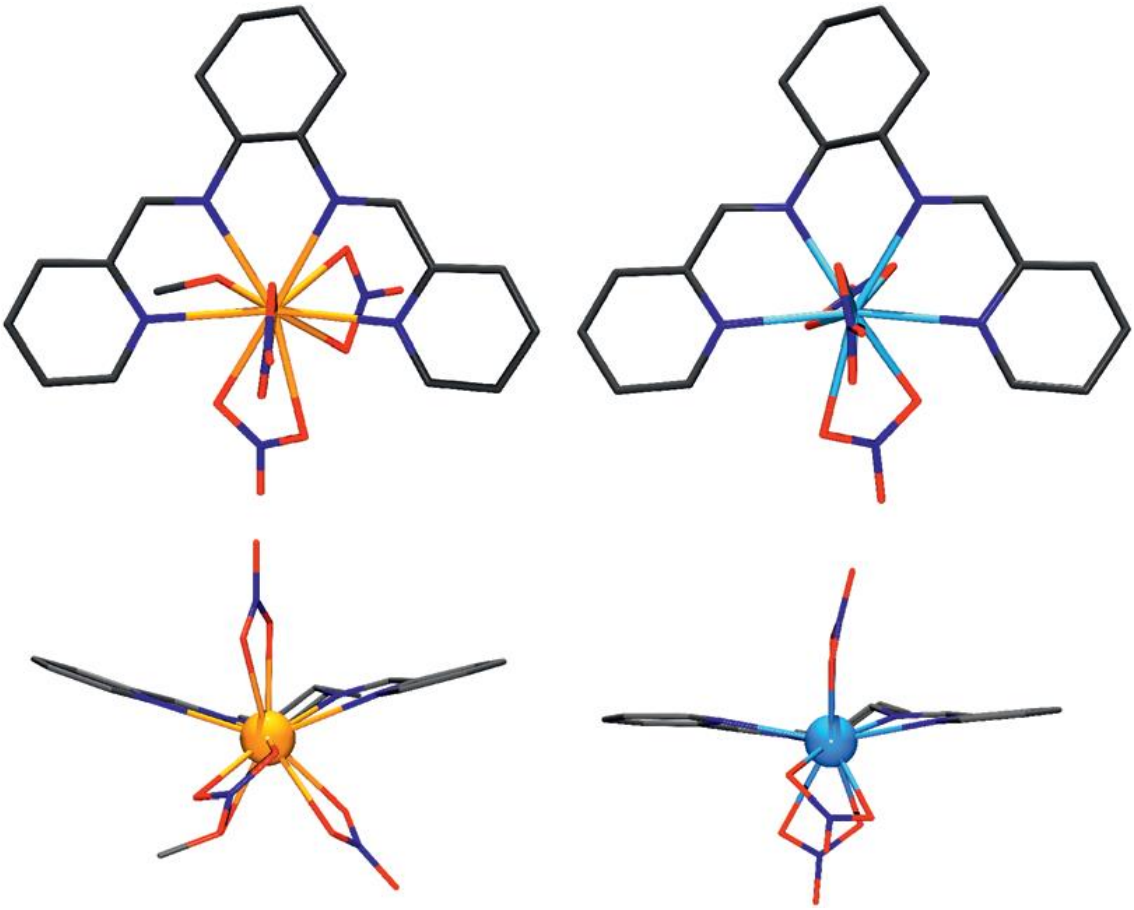

Figure 3

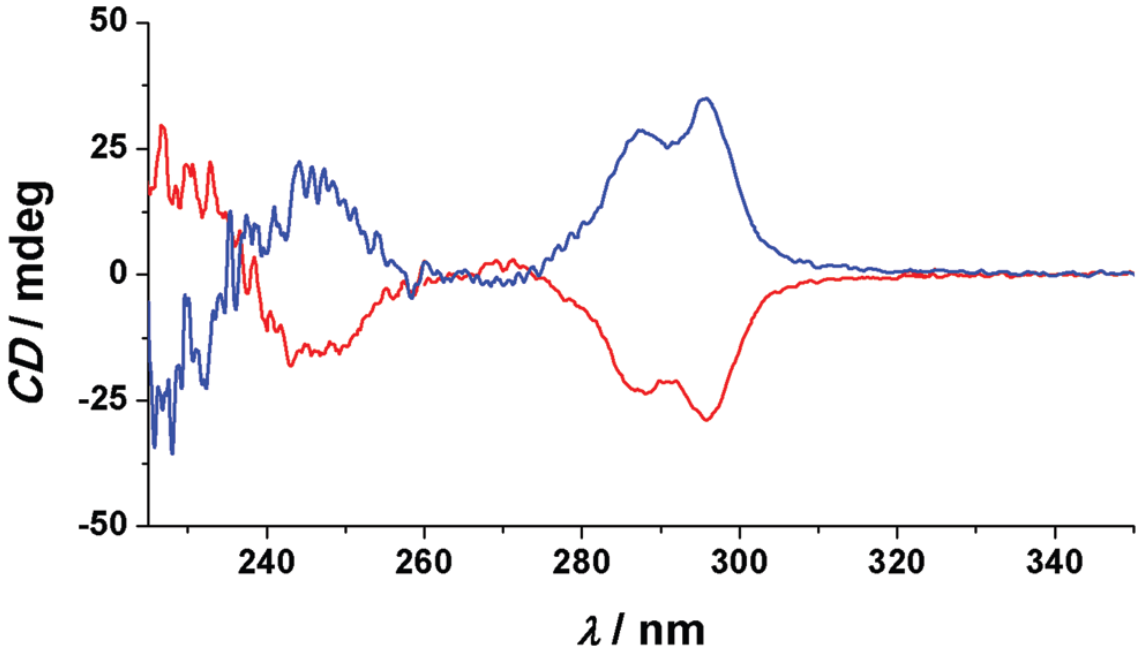

Figure 4

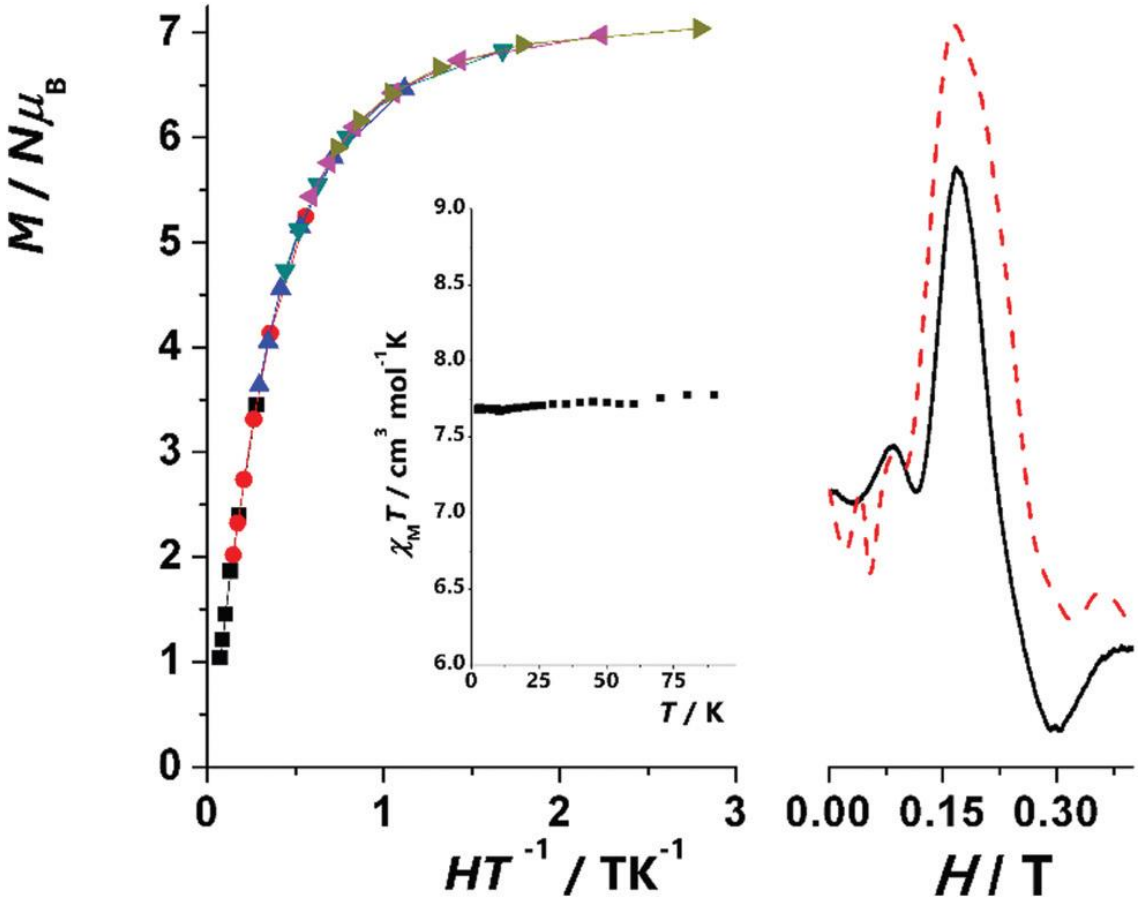

Figure 5

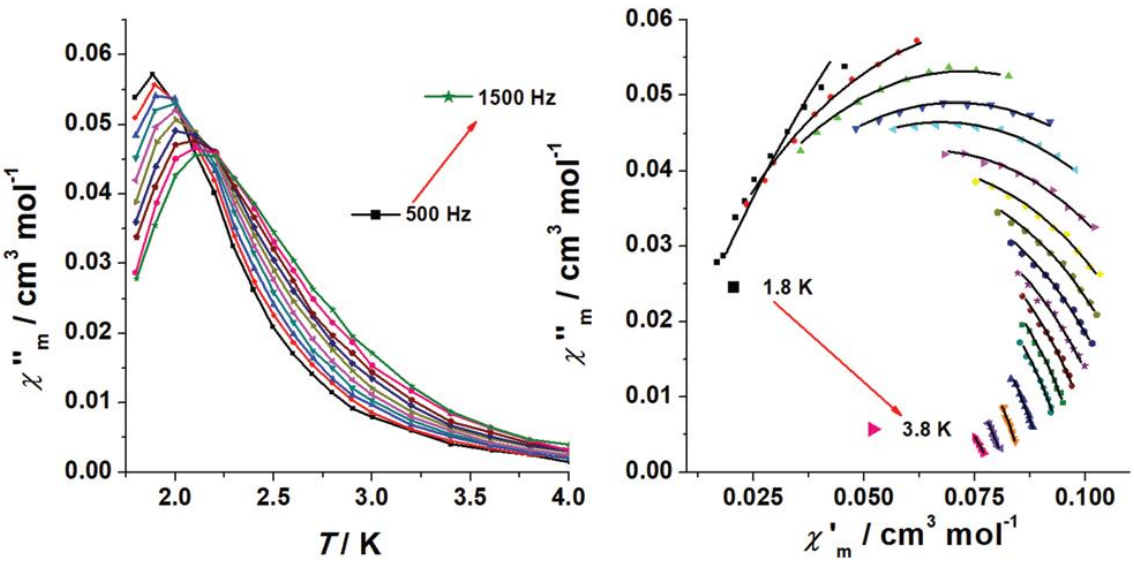
0.06
0.05
0.04
0.03
0.02
0.01
0.00
2.0
2.5
3.0
3.5
4.0
T / K
χ'' m / cm3 mol-1
1500 Hz
500 Hz
0.06
0.05
0.04
0.03
0.02
0.01
0.00
0.025
0.050
0.075
0.100
χ' m / cm3 mol-1
1.8 K
3.8 K

Figure 6

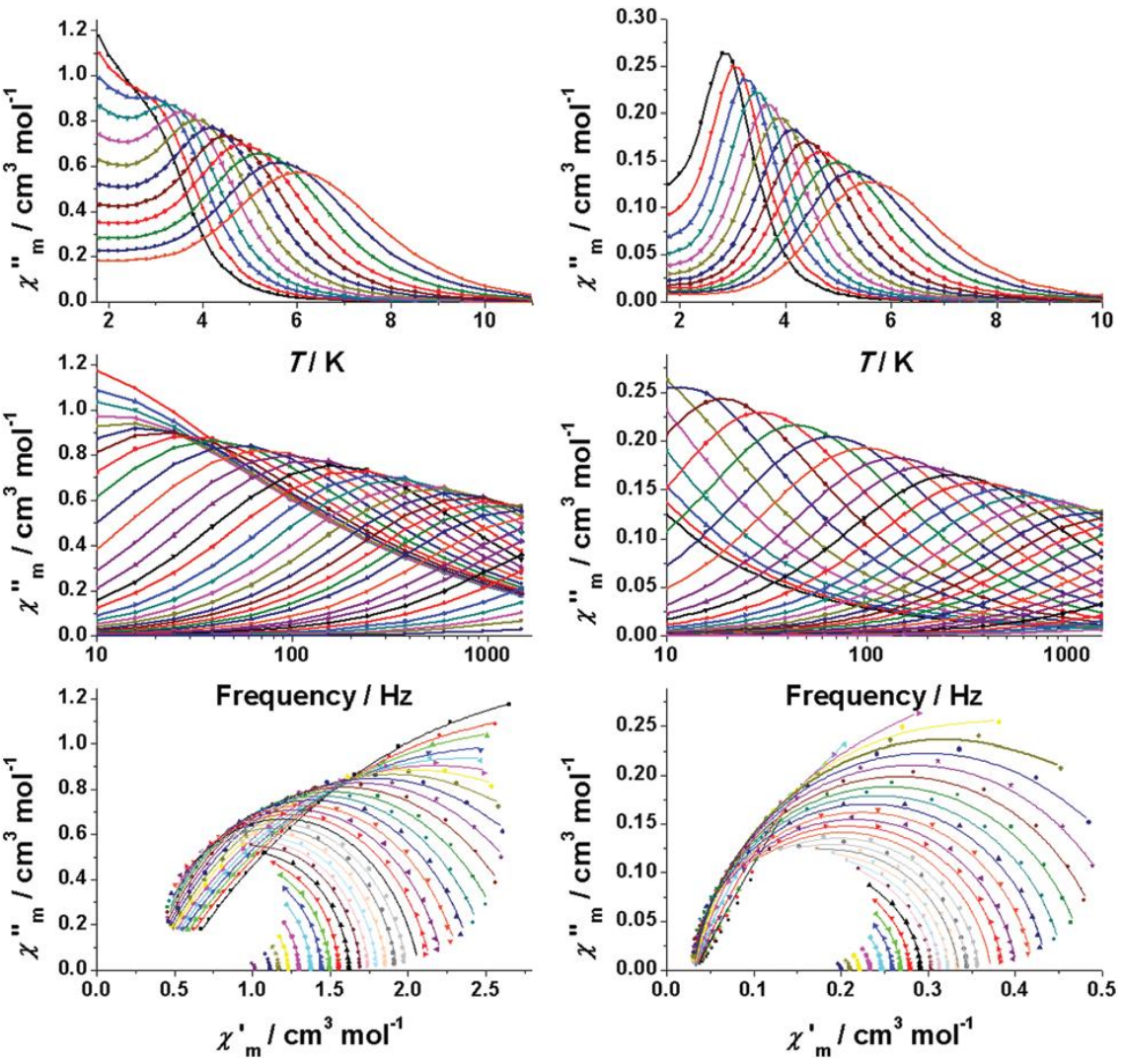

Figure 7

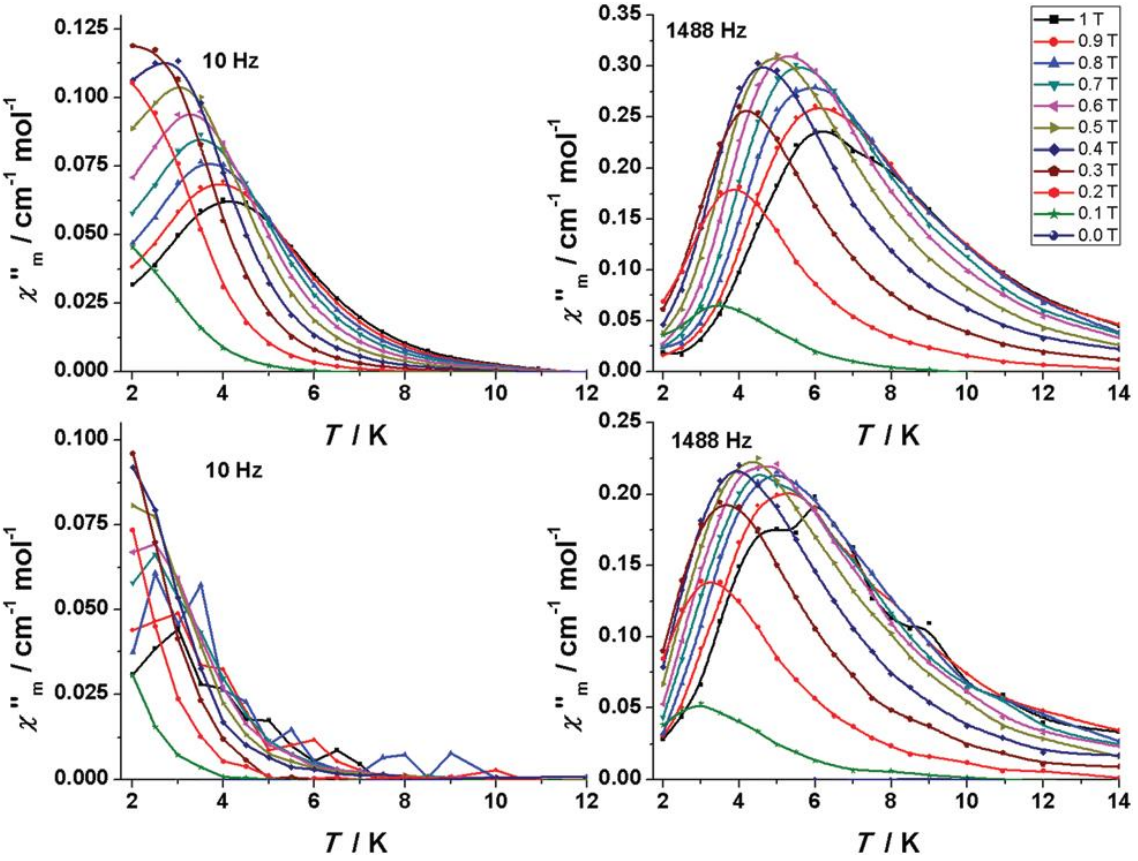
10 Hz
1488 Hz
10 Hz
1488 Hz
1 T
0.9 T
0.8 T
0.7 T
0.6 T
0.5 T
0.4 T
0.3 T
0.2 T
0.1 T
0.0 T
χ'' m / cm-1 mol-1
T / K

Figure 8

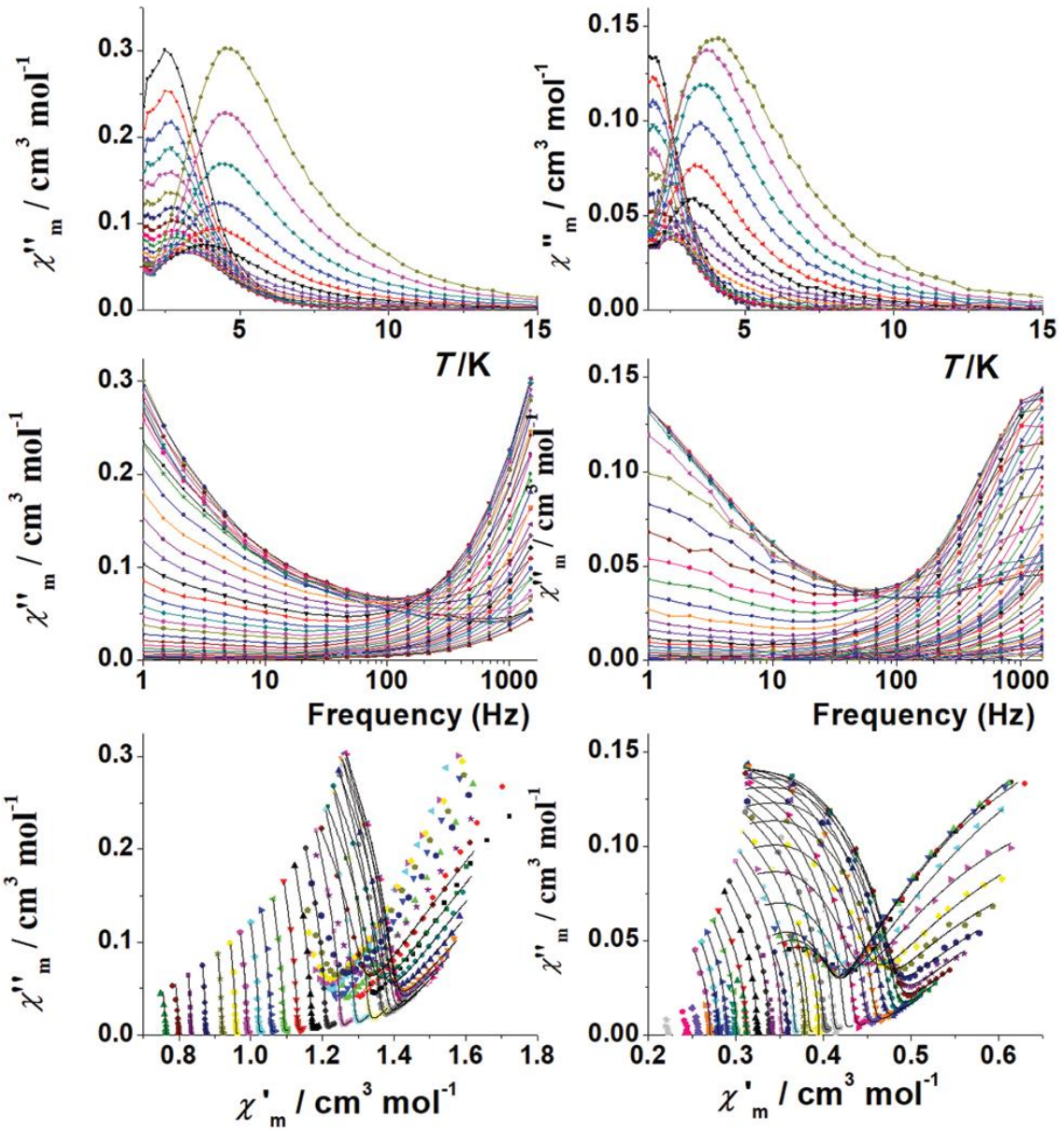

Figure 9